Received 5 March 2009
Revised 30 June 2009
Accepted 29 July 2009

Experimental and numerical investigation of isothermal flow in an idealized swirl combustor

A.C. Benim
Department of Mechanical and Process Engineering, Düsseldorf University of Applied Sciences, Düsseldorf, Germany
M.P. Escudier
Department of Engineering, University of Liverpool, Liverpool, UK
A. Nahavandi
Department of Mechanical and Process Engineering, Düsseldorf University of Applied Sciences, Düsseldorf, Germany
A.K. Nickson
Department of Engineering, University of Liverpool, Liverpool, UK
K.J. Syed
Alstom (Switzerland) Ltd., Birr, Switzerland, and
F. Joos
Laboratory of Turbomachinery, Helmut Schmidt University, Hamburg, Germany

Abstract

Purpose – The main purpose of the paper is the validation of different modelling strategies for turbulent swirling flow of an incompressible fluid in an idealized swirl combustor.

Design/methodology/approach – Experiments have been performed and computations carried out for a water test rig, for a Reynolds number of 4,600 based on combustor inlet mean axial velocity and diameter. Two cases have been investigated, one low swirl and the other high swirl intensity. Measurements of time-averaged velocity components and corresponding rms turbulence intensities were measured using laser Doppler anemometer, along radial traverses at different axial locations. In the three-dimensional, unsteady computations, large eddy simulation (LES) and URANS (Unsteady Reynolds Averaged Navier-Stokes Equations or Reynolds Averaged Numerical Simulations) RSMs (Reynolds-stress models) are basically employed as modelling strategies for turbulence. To model subgrid-scale turbulence for LES, the models due to Smagorinsky and Voke are used. No-model LES and coarse-grid direct numerical simulation computations are also performed for one of the cases.

Findings – The predictions are compared with the measurements and reveal that LES provided the best overall accuracy for all of the cases, whereas no significant difference between the Smagorinsky and Voke models are observed for the time-averaged velocity components.

Originality/value – This paper provides additional valuable information on the performance of various modelling strategies for turbulent swirling flows.

Keywords Turbulent flow, Modelling, Turbines

Paper type Research paper

International Journal of Numerical Methods for Heat & Fluid Flow
Vol. 20 No. 3, 2010
pp. 348-370

0961-5539
DOI 10.1108/09615531011024084

1. Introduction

Accurate calculation of the mean and turbulence flow fields within a swirl-stabilized gas-turbine combustor still represents a major challenge more than 30 years after Jones and Launder (1972) introduced the k-ε turbulence model for the prediction of turbulent

shear flows. In the intervening period, for modelling turbulent flows in general, there has been a shift toward Reynolds stress models (RSM), algebraic stress models (ASM), more recently to large eddy simulation (LES) and finally to direct numerical simulation (DNS). Even for the isothermal situation with which this paper is concerned, DNS is by far still not a practical proposition, whereas LES has already been used to simulate high Reynolds number reacting flow in a combustor geometry (see e.g. Kim *et al.*, 1999; Selle *et al.*, 2004). For turbulent swirling flows, although turbulent viscosity-based two-equation models (TVM) such as the k-ε model have continued to be developed and used (e.g. Xia *et al.*, 1997; Yaras and Grosvenor, 2003), the majority of recent calculations of intensely swirling flows have been carried out using ASM (e.g. Weber *et al.*, 1990) and RSM (e.g. Hogg and Leschziner, 1989; Jakirlic *et al.*, 2004). A recent analysis of turbulent swirling flows by RSM was presented by Jawarneh and Vatistas (2006), where a good agreement with measurements was reported, based, however, on data at a single measuring station. On the other hand, since a first order upwind discretization scheme was used for the momentum equations (Jawarneh and Vatistas, 2006), the role of the artificial diffusion casts a cloud over the achieved agreement.

In TVM (Peyret, 2000) proportionality between the strain rate tensor and the Reynolds stress tensor through a scalar turbulent viscosity is assumed. However, in turbulent swirling flows, the Reynolds stresses are so strongly influenced by flow curvature and pressure gradient that such a proportionality cannot be presumed (Sloan *et al.*, 1986). This flow structure, where an "isotropic" turbulent viscosity is inappropriate, will be referred to as "non-isotropic" in the following, which should not be confused with the isotropicity which refers to the equality of the diagonal components of the Reynolds stress tensor. This deficiency of TVM calls for the application of RSM, which can principally capture non-isotropic turbulence structures. Thus, as mentioned above, in recent times, RSM has been widely used in modelling turbulent swirling flows.

To the best of the authors' knowledge, the application of RSM to turbulent swirling flows (Hogg and Leschziner, 1989, Jakirlic *et al.*, 2004) has been performed within the framework of conventional, steady-state, RANS formulations (RANS is the acronym for Reynolds Averaged Navier-Stokes Equations, or, sometimes, for Reynolds Averaged Numerical Simulations). However, as recently demonstrated (Benim and Nahavandi, 2003), RSM can also lead to serious errors for some highly swirling turbulent flows, when applied within the framework of RANS. The reason seems to be that the low frequency unsteady motion of coherent structures, which can play an important role in turbulent swirling flows, cannot adequately be represented by RSM applied within the framework of RANS (or by any other RANS-based turbulence model).

Therefore, the application of RSM within the framework of an URANS (Unsteady RANS) formulation has been proposed by Benim *et al.* (2005) and employed to investigate the flow reported by Escudier and Keller (1985). Since the unsteady flow mentioned above is intimately related to three-dimensionality (3D), the URANS RSM formulation needs to be applied within the framework of a 3D formulation, even if the flow geometry and boundary conditions are axisymmetric and in steady-state (apart from turbulent fluctuations). LES was also identified (Benim *et al.*, 2005) as potentially capable of accurately predicting turbulent swirling flows, as the non-isotropic turbulence structures are known to be dominant in the large scales, which are resolved.

Recently, an URANS analysis of turbulent swirling flows based, however, on a TVM, i.e. the realizable k-ε model (Shih *et al.*, 1995), was presented by Guo *et al.* (2009). In that study, the main emphasis was, however, not a comparison with experiments but rather a numerical parametric study. In the presented comparison, the rather

unsatisfactory agreement observed between the experiments and predictions (Guo *et al.*, 2009) was attributed to the uncertainties in the experimental inlet conditions.

In the present study, new measurements, and further computations for validation purposes are reported for flow through a new test facility which is based on the geometry of an industrial combustion chamber. The URANS RSM (based on RSM) and LES (based on a Smagorinsky subgrid-scale (SGS) model) methods are again used as the main tools of investigation. In order to take better account of the rather low Reynolds number, which are more dominant for the present test rig, the model of Voke (1996) is also used as the SGS model in LES. For investigation purposes, "no-model" LES (Kawamura and Kuwahara, 1984) and a "coarse-grid" DNS computations are also performed, for one of the cases.

As in the earlier paper of Xia *et al.* (1997), particular consideration is given to the inflow: rather than assuming a prescribed set of inlet conditions, flow through the swirl generator itself is calculated to provide the swirling inflow state. The low Reynolds number k-ε model of Launder and Sharma (1974) is employed to treat the low Reynolds number flow in that area.

As is well known (Escudier and Keller, 1985), the downstream flow conditions play a very important role in swirling flows, which exhibit a subcritical state downstream. Thus, special care is also paid to modelling the outlet boundary accurately.

2. Experimental details

Experiments were carried out for water flow through the idealized model combustor shown schematically in Figure 1. The swirl generator itself, shown schematically in Figure 1b, is based upon the tangential-inlet (slit-tube) design used by Escudier *et al.* (1980) but with the single wide slit used in their arrangement replaced by 12 narrow slits at 30° intervals. The slits were created using 12 identical wedges assembled around a central vertical axis. The wedges were machined from stainless steel and the width of each slit is 1 mm. The outer diameter of the wedge assembly is 165 mm and the inner channel created by the wedges is a dodecahedron with distance between opposing flat surfaces 55 mm. The open axial length of the slits can be varied between 27 and 263 mm by adjusting the axial position of a close-fitting central piston the cross-section of which is also a dodecahedron. The degree of swirl is adjusted by controlling the open slit exit area through a movable central piston. For a given mass flow rate, a large slit exit area (low piston position, long free axial slit length) leads to a low slit exit velocity and so low swirl (LS) whereas a small slit exit area (high piston position, short free axial slit length) leads to a high slit exit velocity and high swirl (HS). The swirl generator is surrounded by a cylindrical jacket of inner diameter 305 mm into which water is fed through six equally spaced 31 mm diameter inlet ports each angled to be tangential to the periphery of the wedge assembly and located half way along its length. The water is fed under gravity from a large (ca. 99,000 l) tank some 36 m above the vortex generator, the flow rate being controlled by two needle valves arranged in parallel.

As shown in Figure 1, the combustor inlet diameter is 50 mm and the inlet is located 65 mm downstream of the swirl generator exit. The body of the combustor itself has an initial diameter of 100.4 mm which after a length of 170 mm tapers over a distance of 125 mm to a diameter that can be adjusted to obtained different exit contractions (Figure 1). In the present work, the configuration with an exit diameter of 35 mm is considered. The entire model is vertical with upward flow discharging from the outlet tube into a large collection tank within which the water level is below that of the outlet

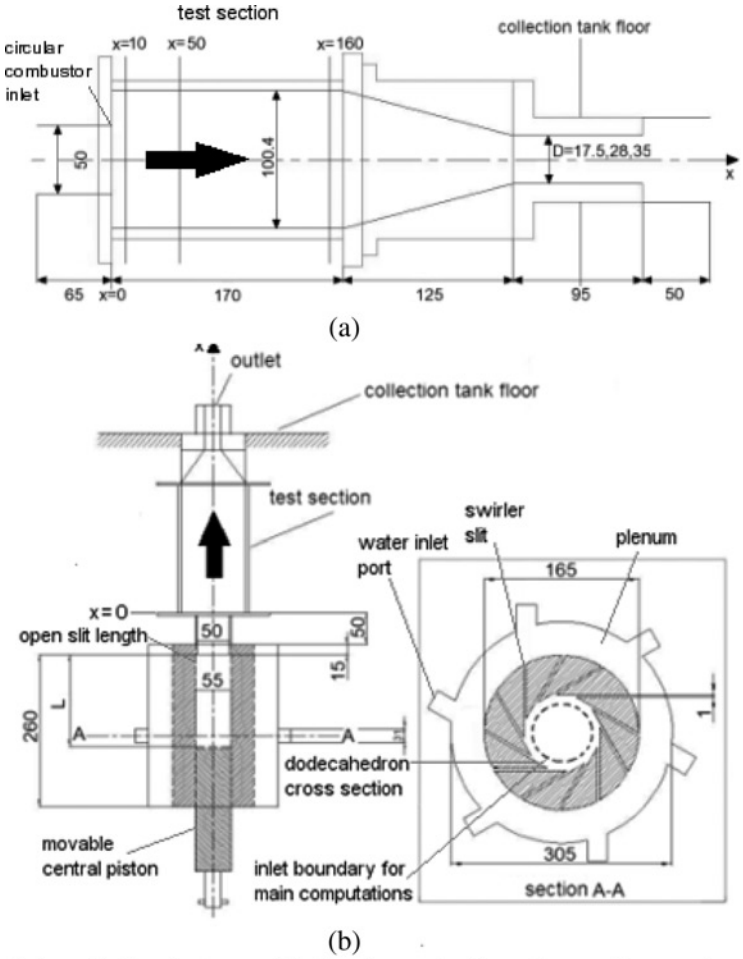

Notes: (a) Combustor model showing main dimensions and measuring planes (in reality the axis of model is vertical with bulk flow upwards); and (b) swirl generator (all dimensions in mm)

Figure 1.
Schematic diagram of experimental set-up

tube so that the experimental outlet condition is that of a free surface at constant (atmospheric) pressure.

Radial distributions of the mean axial (u) and swirl (w) velocity components, and the corresponding rms turbulence intensities (u' and w') were measured in forward-scatter using a Dantec Fibreflow laser Doppler anemometer (LDA) system comprising a 60X10 probe and 57X08 receiving optics. The beam separation at the front lens was 51.5 mm and the lens focal length 160 mm which produced a measuring volume 280 μm in length and 45 μm in diameter. The axial measurement locations, shown in Figure 1, were $x = 10$, 50 and 160 mm, where the axial distance x is measured from the inlet to the combustor. Flow rates were determined by measuring the volume of water flowing through the rig over a measured period of time. For the detailed measurements reported here, the flow rate was set to achieve a Reynolds number of 4,600 based on the bulk axial velocity and diameter at the combustor inlet. Higher flow rates resulted in

gaseous cavitation within the low-pressure central core of the swirling flow so that LDA measurements were no longer possible. The resulting flows were found nevertheless to be turbulent at this Reynolds number.

3. Computational details

The numerical analysis is based on the commercial general-purpose CFD code ANSYS-CFX (ANSYS-CFX, 2006), in which the continuity and Navier-Stokes equations are treated by a coupled solver and a finite volume discretization is applied to the governing equations in conjunction with an unstaggered, unstructured grid definition.

3.1 URANS RSM

The acronym URANS stems from "Unsteady RANS". Within the framework of URANS, the contribution of the random turbulent fluctuations is expressed through the "Reynolds stresses", which need to be described by a statistical turbulence model. Applying the RSM as the statistical turbulence model, each of the six independent components of the symmetric Reynolds stress tensor is obtained by solving its own transport equation. As applied here, in the "modelled" transport equation for the Reynolds stresses, the anisotropic diffusion coefficients of the original equations are replaced by an isotropic approximation (ANSYS-CFX, 2006). For the pressure-strain correlation term, the modelling approach of Speziale *et al.* (1991) has been adopted. This approach was demonstrated (Grotjans *et al.*, 1999) to be clearly superior, especially for strongly rotational flows, to the alternative formulation of Launder *et al.* (1975). In addition to the six Reynolds stress transport equations, an additional transport equation has to be solved for the dissipation rate of turbulence kinetic energy ε. In all modelled transport equations, default model constants are used (ANSYS-CFX, 2006).

For URANS RSM, the advection terms in the momentum equations are discretized by the so-called high-resolution scheme (Barth and Jespersen, 1989), which achieves maximum possible accuracy between first and second order, without violating boundedness. For the advection terms of the transport equations for the Reynolds stresses and the dissipation rate of the turbulence kinetic energy, an upwind difference scheme (Peyret, 2000) is applied (due to the more favourable convergence behaviour compared to a higher order discretization).

3.2 LES

Within the framework of LES, the correlation tensor, i.e. the SGS stress tensor, resulting from the filtering operation needs to be modelled (Sagaut, 2002). Quite frequently this is done by means of an SGS eddy viscosity ν_{SGS} that defines the proportionality between the deviatoric part of the SGS stress tensor and the resolved strain rate tensor. For determining the SGS viscosity, the Smagorinsky model (Smagorinsky, 1963) is basically used in the present work, which is a mixing-length-like model approximating the SGS viscosity by means of a length scale (filter width) and the resolved strain rate tensor. The filter width is taken to be proportional to the mesh size, the proportionality constant being the Smagorinsky coefficient, which is assumed to have the constant value of 0.1, a commonly used value. It would be of interest to investigate the effect of varying the value of this constant but this was precluded due to resource limitations. A dynamic SGS model might have advantages but this was not possible within the capabilities of the code used.

It has been mentioned already that the Reynolds numbers of the flows investigated here are somewhat low, and certainly lower than in practical combustors. In the

literature it is argued (Sagaut *et al.*, 2000) that the Smagorinsky model does not represent the correct asymptotic behaviour with decreasing Reynolds number and in this sense the model of Voke (1996) is considered to be an improvement over Smagorinsky's. Voke (1996) computes an SGS viscosity ($\nu_{SGS,VO}$) that takes low Reynolds number effects into account by reducing the SGS viscosity of the standard Smagorinsky model ($\nu_{SGS,SMG}$) according to:

$$\nu_{SGS,VO} = \nu_{SGS,SMG} - \beta\,\nu\left[1 - exp\left(-\frac{\nu_{SGS,SMG}}{\beta\,\nu}\right)\right] \tag{1}$$

where the constant $\beta = 2/9$ was based on fitting to eddy viscosity estimates that are in agreement with Pao's dissipation spectrum (Pao, 1965) and the variable ν denoting the molecular kinematic viscosity. This model is implemented in ANSYS-CFX (2006) and applied in the simulation of the flows considered here.

For both SGS models, the SGS viscosity is explicitly brought to zero in the vicinity of solid boundaries by applying a Van Driest damping function (Van Driest, 1956):

$$\nu_{SGS} = \nu_{SGS,0}\left(1 - exp\left(-\frac{y^+}{A^+}\right)\right) \tag{2}$$

where $\nu_{SGS,0}$ denotes the undamped SGS viscosity obtained by one of the two models described above, and ν_{SGS} is the SGS viscosity after damping. In (2), A^+ is a constant ($A^+ = 25$) and y^+ is the non-dimensional wall distance ($y^+ = y\sqrt{\tau_w/\rho}/\nu$, where y is distance from the wall, ρ the density, and τ_w the wall shear stress).

In LES, the central differencing scheme (Peyret, 2000) is used for discretizing the advection terms of the momentum equations, in order to prevent the SGS model being influenced by the artificial diffusion introduced by the high resolution scheme.

3.3 "No-model" LES and "coarse-grid" DNS

The similarity between the numerical dissipation and the SGS viscosity models has led certain researchers to perform "no-model" LES (NM LES), where the filtering is based entirely on the numerical method (Kawamura and Kuwahara, 1984). Here, the artificial diffusion introduced by the discretization scheme is assumed to completely replace the SGS viscosity. Thus, the model employs no explicit SGS model. The performance of this NM LES approach is also investigated for one of the test cases here: the high-resolution scheme (Barth and Jespersen, 1989) is used in discretizing the advection terms of the momentum equations, which introduces an optimal amount of numerical dissipation.

As a further trial "coarse-grid" DNS (CG DNS) computations are also performed for some cases, using the same grid as for LES, but without applying any SGS model or introducing any numerical dissipation. The difference between this CG DNS and NM LES is in the use of the non-dissipative central differencing scheme to discretize the advection terms in CG DNS, instead of the dissipative high-resolution scheme used for NM LES.

3.4 Boundary conditions

3.4.1 The inlet boundary. As described earlier, the swirl generator consists of 12 identical wedges assembled around a vertical axis, leaving 1 mm slits in between, resulting in a dodecahedron-shaped cross-section, with distance between opposing flat surfaces 55 mm (Figure 1). The combustor inlet has a circular cross-section with a slightly smaller diameter of 50 mm. The "imaginary" cylindrical surface, which would

be created by an "extrusion" of the circular combustor inl*et al*ong the swirl generator axis, into the swirl generator is defined to be the inlet boundary of the solution domain. The circular cross-section of this inlet surface, which is placed slightly downstream of the outlets of the dodecahedron-shaped outlet of the swirl generator is indicated by a dashed line in Figure 1b (right).

To determine the swirling inlet conditions, preliminary RANS computations were performed for the inlet section, i.e. for a solution domain incorporating the plenum, the slits and the swirl generator. 3D computations were performed for a wedge-shaped solution domain covering a single slit, i.e. one- twelfth of the whole circumference, applying periodic boundary conditions on the boundaries in the circumferential direction. For different positions of the central piston, 3D block-structured grids with about 500,000 hexahedral cells were employed to discretize the domain. The flows in the individual slits are practically laminar with slit Reynolds numbers (based on the slit width and the bulk velocity corresponding to the free slit area), ranging between 60 and 500 depending on the bulk flow rate. Since turbulence develops in the swirl generator, the low Reynolds number k-ε model of Launder and Sharma (1974) is used as the turbulence model in these preliminary computations to cope with this situation. Hereby, special care was taken to ensure a sufficiently fine resolution of the near-wall regions, fulfilling the condition of $y^+ \leq 1$ for the near-wall cells, which is necessary for a proper use of the turbulence model employed. The results obtained along the cylindrical surface, which is defined to be the inlet boundary for the main computations, have shown quite smooth distributions along the circumference with deviations smaller than ±4 per cent from the circumferentially averaged values. Thus, it is concluded that the inlet conditions for the main computations, to be prescribed on the above-mentioned cylindrical surface, can be assumed to be circumferentially uniform, without a substantial loss of accuracy. These are obtained by circumferentially averaging the results of the preliminary computations, along the cylindrical combustor inlet surface. The resulting inlet boundary conditions for the LS and HS cases are displayed in Figure 2, where the variations of the axial (U_o), radial (V_o) and circumferential (W_o) velocity components, along the axial direction are shown (the x direction in Figures 1 and 2 is the same). For LS, the position of the movable central piston (Figure 1) is rather low, leaving a quite long (250 mm) free slit length (Figure 1). This rather low slit exit area contraction leads to quite smooth distributions (Figure 2a). For HS, the piston position is high, which means a rather short free slit length (30 mm) achieved by a sudden area contraction. This causes a comparably inhomogeneous flow field (Figure 2b).

The preliminary simulations of the inlet section did not indicate any turbulence generation at the position of the cylindrical inlet boundary. In order to be confident about the accuracy of the inlet boundary conditions for the velocities, the computations for the inlet section were repeated assuming laminar flow which resulted in practically the same profiles (Figure 2) being obtained.

Thus, the same, steady-state velocity boundary conditions are applied for all models, including LES. The inlet boundary conditions for the turbulence quantities, which are additionally required by URANS RSM computations are derived by assuming a very low turbulence intensity (0.1 per cent) and a very low turbulence to laminar viscosity ratio (0.1 per cent) at the inlet boundary. The prescribed too low turbulence levels (for coping with the flow physics) may be thought to be not ideally suited to the RSM model employed. However, it has been observed that variations of the inlet turbulence in reasonable ranges did not lead to a substantial change of the results in the combustor.

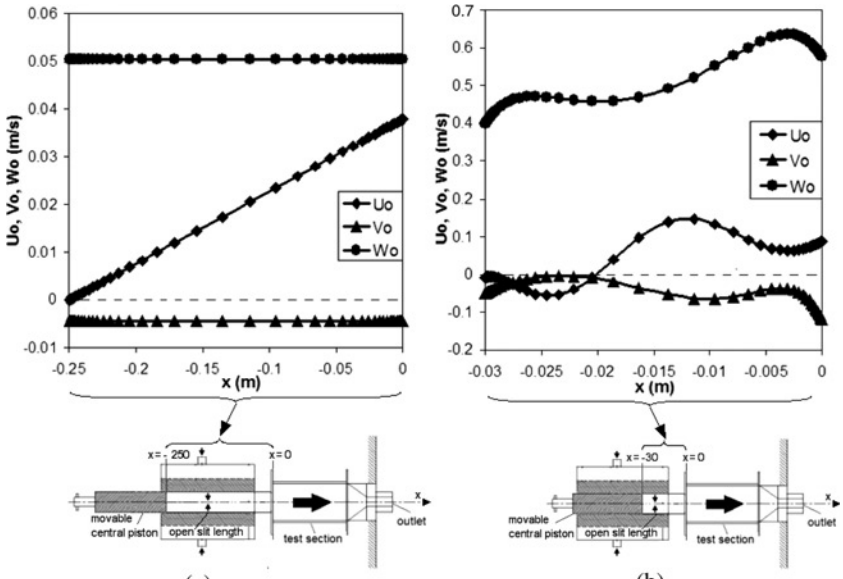

Notes: (a) LS and (b) HS

Figure 2.
Inlet boundary conditions

3.4.2 Wall boundaries. At all solid surfaces, no-slip boundary conditions are applied. In the applied turbulence models, the viscosity-affected sublayer region near any wall is bridged by empirical formulas, i.e. by the so-called "wall functions" (Launder and Spalding, 1974). Generally speaking, the wall functions are not ideally suited to LES. Nevertheless, we assume that any inaccuracy that occurs in near-wall regions does not cause a substantial deterioration of the LES predictions, since the flow structures which are important here, such as the internal recirculation zone, are related to "free shear layer" effects rather than being "wall driven".

3.4.3 The outlet boundary. As already stated, the water test rig has a vertical orientation, the main flow direction being vertically upward. The water leaving the duct exits the test section by spilling out radially into a chamber, forming a water layer a few millimetres deep with a free surface. This outlet geometry is modelled as realistically as possible, by letting the solution domain to extend up to the experimentally observed height of the free surface of the water layer, assigning a zero-shear slip boundary condition at this boundary. The small circumferential ring area remaining between the outer edges of the rig wall and the zero-shear boundary (approximating a free surface) is defined to be the outlet boundary, where the water can leave the domain in the radial outwards direction, assigning a constant pressure and zero-gradient boundary conditions for other variables at that boundary.

3.5 Numerical discretization

The schemes employed for the spatial discretization of the convection terms differ from turbulence model to model. These have already been discussed above. For the time discretization, a second order backward Euler scheme (Peyret, 2000) is used. For the success of an unsteady formulation, an adequate choice of the time step is, of course, important. The computations are carried out using a dimensionless time step size (Δt)

of $\Delta t = 5 \times 10^{-4}$, which is non-dimensionalized by the integral time scale (T_I which has a physical value of about 0.5 s) based on the combustor inlet diameter and bulk velocity.

With this time step, the resulting cell Courant numbers (Peyret, 2000) remained below 0.01 as an average value over the combustor domain, whereas local maximum values remained below 0.8, for all cases. It was observed that the ratio of the time step size to the local Kolmogorov time scale (Hinze, 1959) remained below unity for all cases. Thus, for the present computations, it can be assumed that the temporal resolution was sufficiently accurate.

For the LES computations, the resolution of the turbulence length scales is also a very important issue. For the configurations considered here, the ratio of the local filter width (grid size) to the local Kolmogorov length scale (Hinze, 1959) varied between seven and 14 as an average value over the combustor domain, whereas the local maximum values ranged between 12 and 39 from case to case. Recently, Fröhlich *et al.* (2005) showed that this ratio should be less than ten to obtain DNS-like accuracy in LES computations. On this basis, we assume that the present spatial resolution of turbulence scales can be considered to be reasonably accurate for the LES computations.

3.6 Computational grids

A conformal block-structured grid generation strategy based on hexahedral finite volumes was applied. Although a 3D grid independency study has not been performed, the 3D grid employed here is based on a preliminary grid independency study performed for a two-dimensional (2D)-axisymmetric, steady-state analysis. The surface grids of the 3D grids for the "LS" and "HS" cases are shown in Figures 3a and b, in perspective view.

A longitudinal section of the 3D grid in detail view near combustor inlet is shown in Figure 4a. As seen in the figure, the aspect ratios of the cells are very close to unity in the inlet section of the combustor, where vortex breakdown is expected. In generating the 3D grid based on the previous 2D grid, the number of cells in the circumferential direction is adjusted in such a way that the ratio of the circumferential cell width to the radial cell width was close to unity in the central regions and remained moderate on the combustor wall (aspect ratio below 4). A cross-section of the 3D grid in the combustor is shown in Figure 4b. Each of the generated 3D grids had about 10^6 cells in total.

3.7 The solution strategy

Turbulent viscosity based two-equation turbulence models used initially for 3D URANS were unable to capture unsteady flow behaviour instead converging to a steady-state axisymmetric flow field. The results of these calculations were used as initial conditions. The time-dependent computations were then carried out for a sufficient period of time for unsteady behaviour to fully develop. This was judged by monitoring flow variables at selected points. Thereafter, time averaging of the results was started and continued until the average solution showed no substantial changes in time. Normally the total computation time for each case was about 20 T_I, the first 6 T_I used for the initial settling time and the remaining 14 T_I for the time averaging. Ideally, time averaging should be performed until all flow variables are absolutely constant and, in our case, perfectly axisymmetric. However, it was observed that it can take extremely long to achieve these ideal conditions for some cases and the computations were stopped when the main time-averaged flow structure showed no further substantial changes other than a smoothing at small scale, without substantial

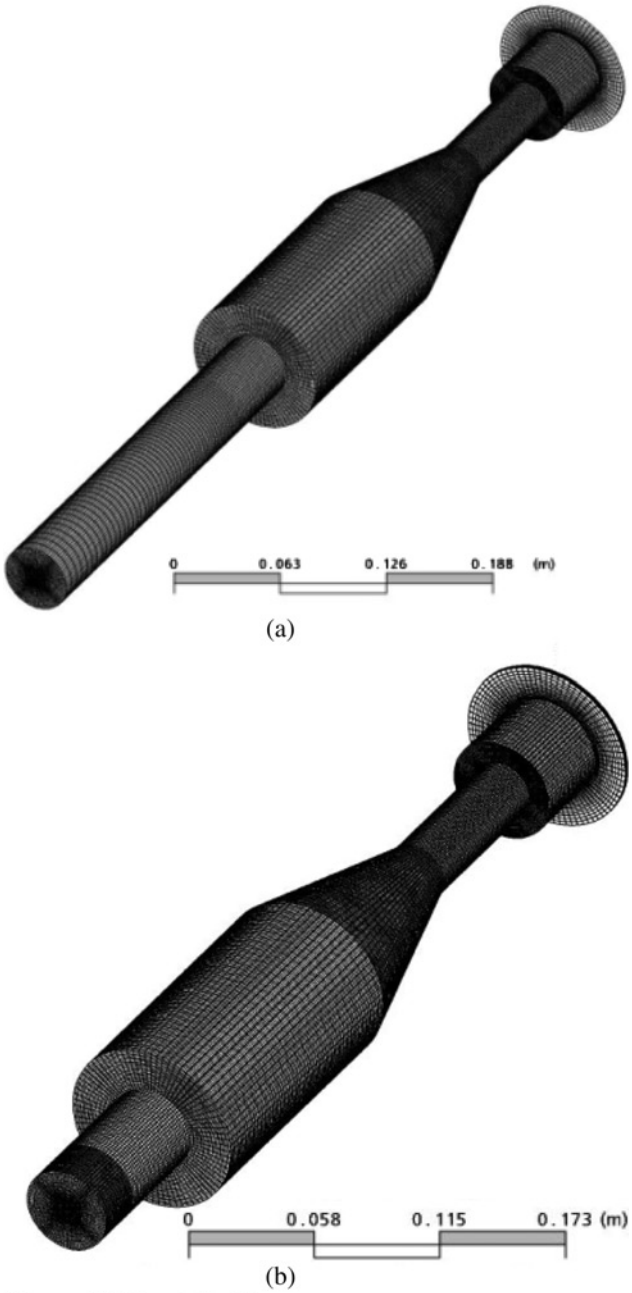

Notes: (a) LS; and (b) HS

Figure 3.
Surface grids

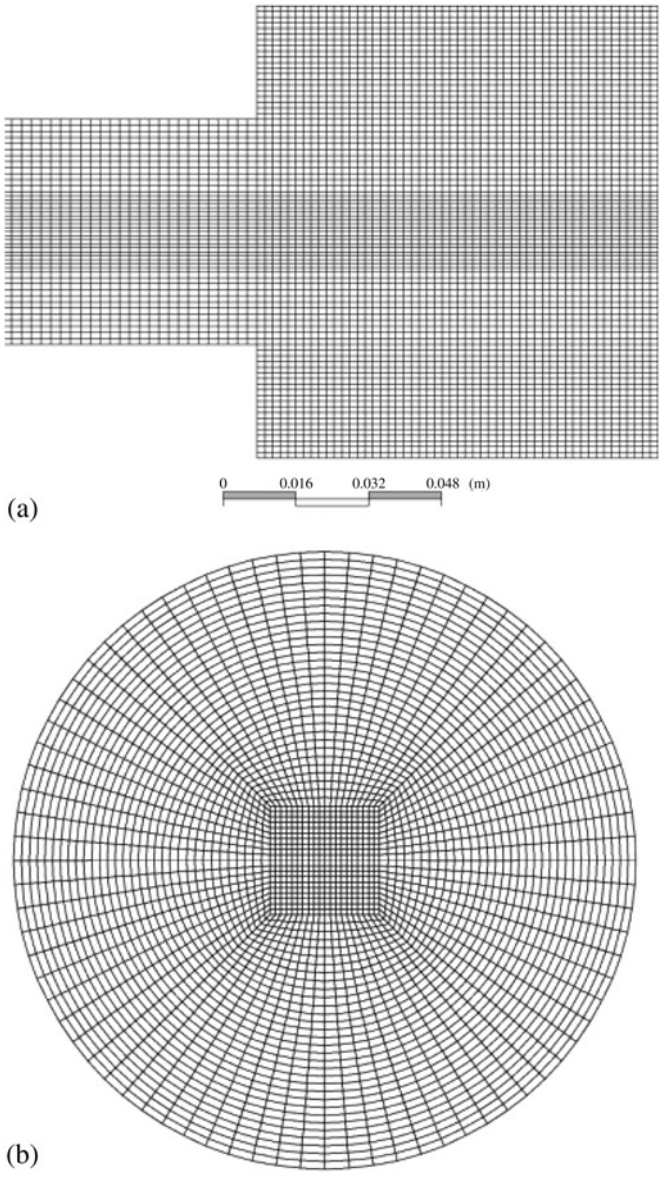

Figure 4.
Different sections of 3D grid

Notes: (a) Longitudinal section, detail near combustor inlet; and (b) cross-sectionat $x = 10$ mm

contributions to the predictive performance of time-averaged profiles (this applies rather to LES, since smooth and stable time-averaged distributions are more easily obtained by URANS). For this reason, the time-averaged results presented here do exhibit some asymmetries and oscillatory behaviour, which we believe, however, do not detract from the main conclusions.

4. Results

It has already been discussed above that the predicted time-averaged velocity field may show some asymmetries. The same is true also for the experimental data (since it would similarly take extremely long to achieve a perfect symmetry by time-averaging the measurements). No averaging of the experimental data on either side of the centreline was performed (which would then "enforce" a perfect symmetry).

4.1 Low swirl

Radial profiles of time-averaged axial velocity at the axial stations $x = 10$, 50 and 160 mm are shown in Figure 5. This figure immediately reveals the complexity of the mean axial flow field. The experimental data show reverse flow at $x = 10$ and 50 mm both on the axis as well as in the corner downstream of the sudden expansion into the combustor. The low-speed central core is surrounded by a high-velocity annular jet and regions of very high shear. By $x = 160$ mm, however, the flow reversals have disappeared completely and been replaced by a strong jet-like overshoot in the central core. The mean flow characteristics are captured reasonably well at $x = 10$ mm by the NM LES and CG DNS calculations which are almost identical while the URANS RSM (indicated by U RSM in the figure) performs poorly producing a slight velocity deficit on the centreline but no flow reversal. Although there are differences between the two LES calculations using the Smagorinsky's (LES Smg) and Voke's (LES Voke) SGS models, both are in similar overall agreement with the experiments. The URANS RSM calculation is again the least satisfactory at $x = 50$ mm and the LES comes closest to the data but fails to capture the full radial extent of the reverse flow. By $x = 160$ mm none of the calculations compares well with the measurements, although once again the LES calculation is the closest and captures the main flow features while the URANS RSM is poor.

For the time-averaged swirl velocity, the LES calculations at $x = 10$ and 50 mm agree well with the data (Figure 6). URANS RSM again compares poorly while the NM LES and CG DNS calculations suggest peak velocities much higher than measured as well as a curious kink in the region of $r/R = 0.5$ for $x = 10$ mm. At $x = 160$ mm none of the calculations agrees particularly well with the data, although LES results are the most satisfactory and URANS RSM the least satisfactory.

Only the URANS RSM and LES calculations are compared with measurements of the rms fluctuations of the axial- and swirl-velocity components (u' and w'), which are shown in Figures 7 and 8, respectively. The rms fluctuations displayed for LES are based on the resolved velocity field, not taking any SGS contributions into account. On the other hand, the fluctuations displayed for URANS RSM stem directly from the computed Reynolds stresses, with no contribution from the unsteadily resolved velocity field. Thus, the meaning of "fluctuations" differs between the three curves (one experimental and two computational), which is an unavoidable drawback of this comparison.

At the first measurement location ($x = 10$ mm) the URANS RSM calculation of u' picks up little of the fine detail and is clearly unsatisfactory, whereas once again the LES calculations are in generally good agreement with the measurements, the greatest discrepancy being at the radial location where u is a maximum ($r/R \approx 0.$). The w' comparison is less satisfactory particularly in the outer recirculating flow ($r/R > 0$) where the w velocity is relatively uniform. The peaks in u' and w' at $r/R \approx 0.5$ are well reproduced by the LES calculations but only just evident in the URANS RSM calculation. The agreement becomes progressively worse with downstream distance,

although at $x = 50$ mm the LES calculations are in broad agreement with the measurements albeit the peaks in u' are some 20 per cent too high, whereas the URANS RSM calculation predicts the peaks to occur closer to the axis than measured and much lower in value. The results of the LES calculations of w' are again closer to the

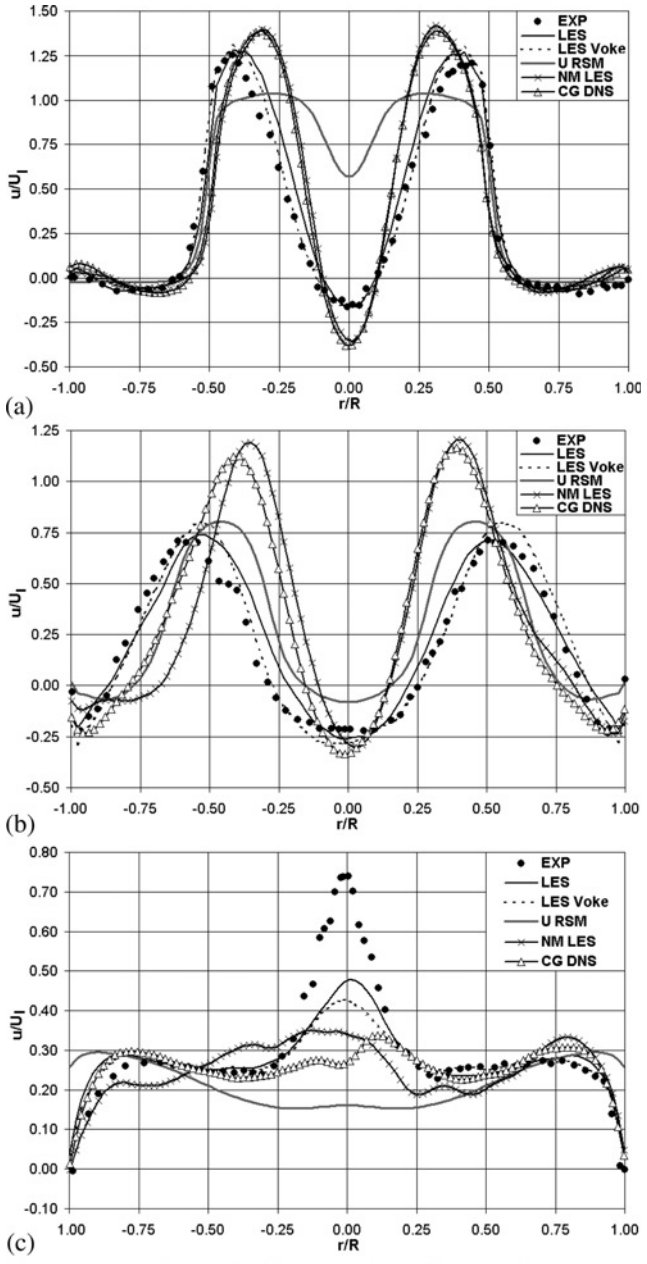

Notes: x = (a) 10 mm, (b) 50 mm and (c) 160 mm (LS)

Figure 5.
Predicted and measured radial distributions of time-averaged axial velocity (u)

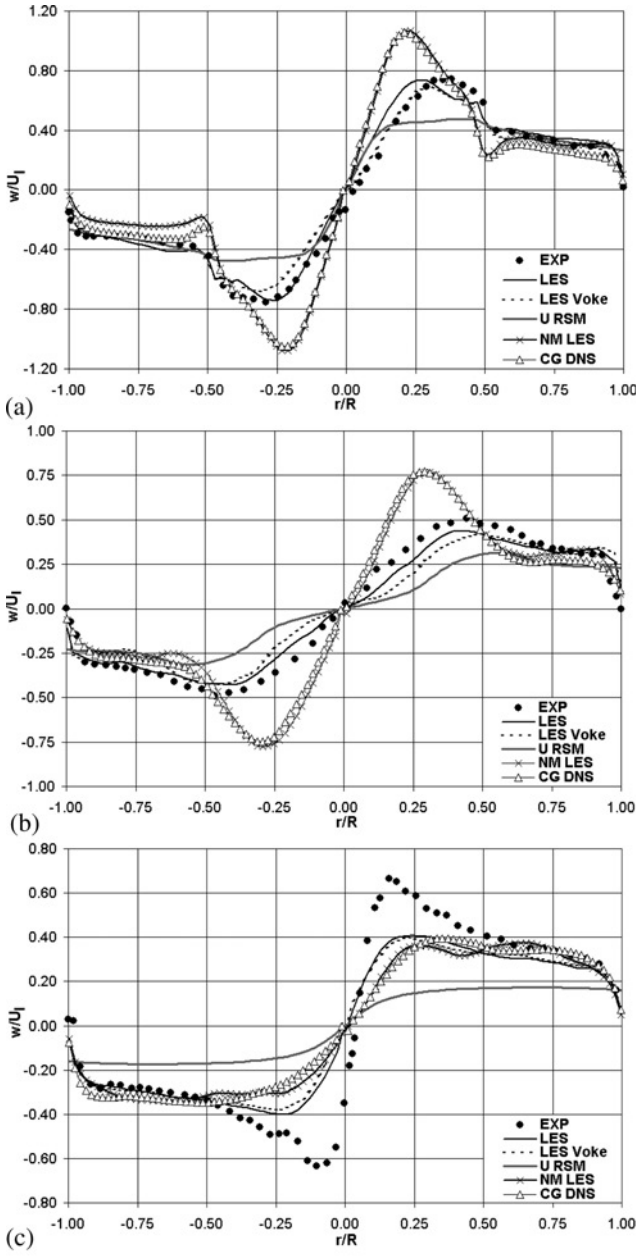

Notes: x = (a) 10 mm, (b) 50 mm and (c) 160 mm for (LS)

Figure 6.
Predicted and measured radial distributions of time-averaged swirl velocity (w)

measurements at $x = 50$ mm than those for the URANS RSM calculation. The w' LES calculation at $x = 160$ mm underpredicts the peak value (close to the axis) by about 40 per cent but is qualitatively in agreement with the data whereas the RSM calculations predicts no peak at all.

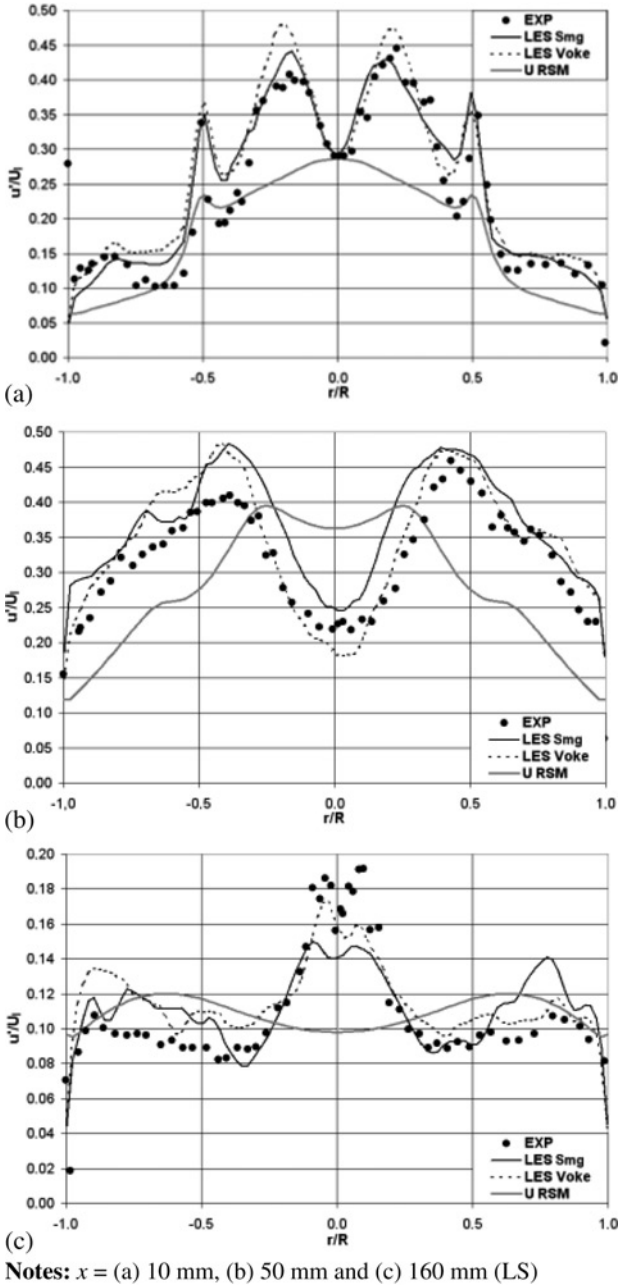

Figure 7.
Predicted and measured radial distributions of rms fluctuations of axial velocity (u')

Notes: x = (a) 10 mm, (b) 50 mm and (c) 160 mm (LS)

4.2 High swirl

The computed and measured time-averaged axial velocity profiles for this case are shown in Figure 9. The most obvious difference between the mean-flow low-contraction axial-velocity data for LS and HS (Figure 9 compared with Figure 5) is that

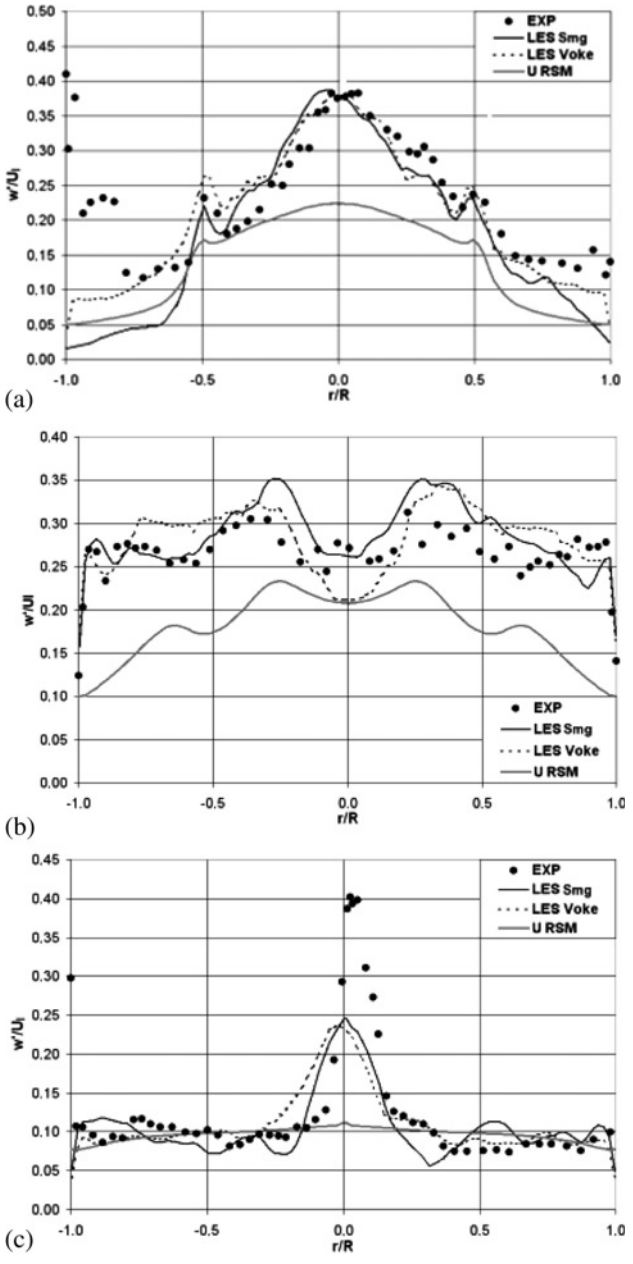

Notes: x = (a) 10 mm, (b) 50 mm and (c) 160 mm (LS)

Figure 8.
Predicted and measured radial distributions of rms fluctuations of swirl velocity (w')

in the latter case there is no flow reversal on the centreline at any x-location. Instead there is peak flow reversal at $r/R \approx 0.3$ at all x-locations. Intense reverse flow is seen at $x = 10$ mm near the outer wall of the combustor but is no longer in evidence at $x = 50$ mm, indicating a much shorter attachment length of the recirculation produced

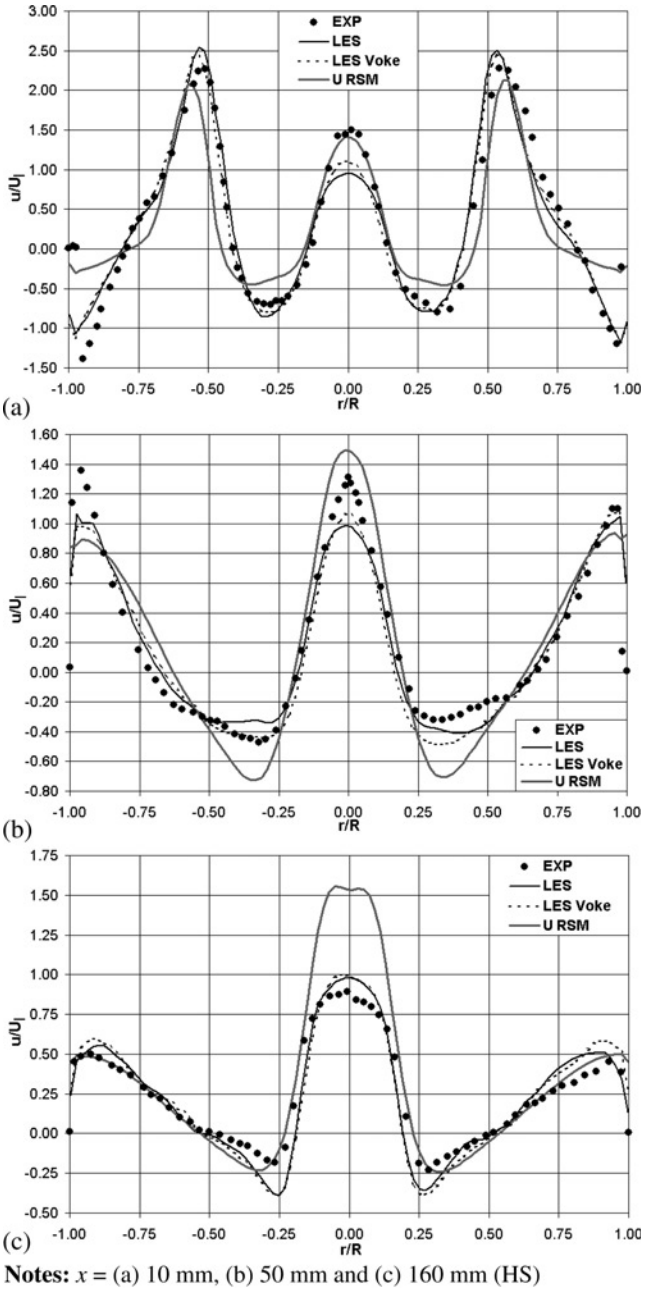

Figure 9.
Predicted and measured radial distributions of time-averaged axial velocity (u)

Notes: x = (a) 10 mm, (b) 50 mm and (c) 160 mm (HS)

by the sudden expansion. Only the URANS RSM and LES calculations are shown and once again the LES calculation produces the most convincing results overall, although in contrast to the LS situation the URANS RSM calculation is superior at $x = 10$ mm at virtually all radial locations. At $x = 50$ mm there is little to choose between the two

calculations, whereas at $x = 160$ mm the LES is clearly superior, particularly in the central overshoot region ($r/R < 0.2$).

For the swirl velocity distributions (Figure 10) there is little to choose between the URANS RSM and LES calculations both of which compare well with the experimental

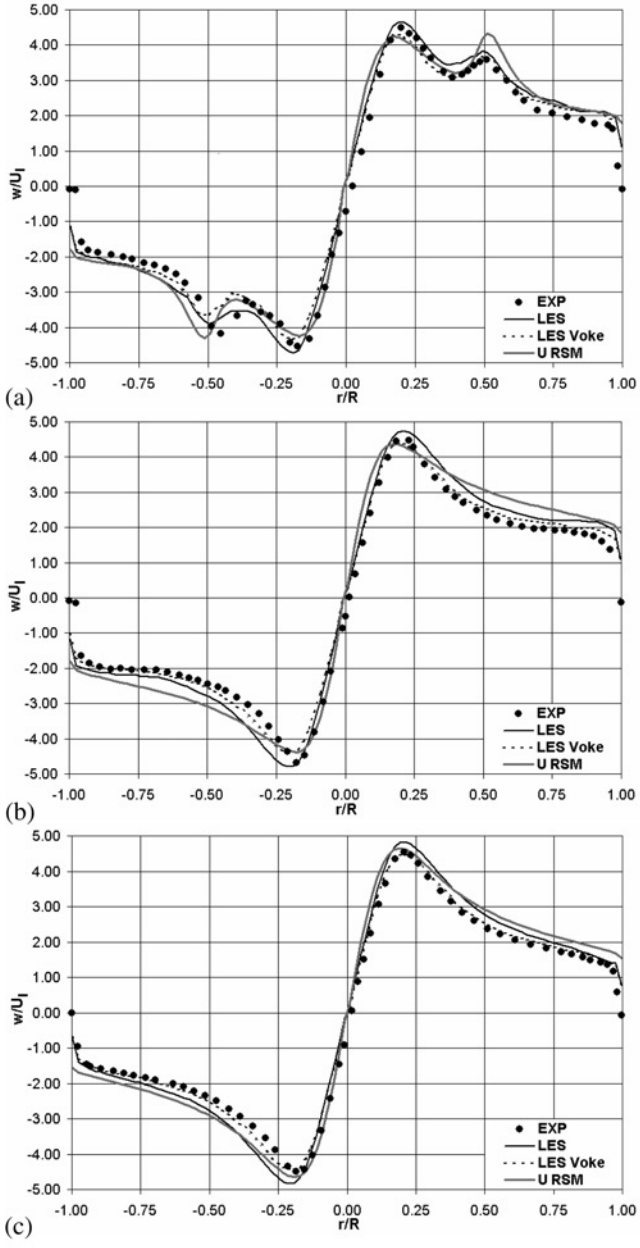

Notes: x = (a) 10 mm, (b) 50 mm and (c) 160 mm (HS)

Figure 10.
Predicted and measured radial distributions of time-averaged swirl velocity (w)

results, although LES still performs somewhat better in non-central regions for $x = 50$ mm. It is interesting to note that the swirl velocity profile exhibits two distinct peaks at $x = 10$ mm, as shown by the experiments and indicated by all predictions.

The comparisons with u' and w' confirm the overall superiority of the LES calculations over the URANS RSM approach (Figures 11 and 12). At $x = 10$ mm the RSM calculation underpredicts the peak u' values by about 50 per cent, although the radial variation of u' is qualitatively satisfactory except, perhaps, close to the outer wall of the combustor. At $x = 50$ mm, once again the LES calculation is in better agreement with the u' data, although the levels are overpredicted by some 30 per cent except in the region close to the axis. The URANS RSM calculations fail qualitatively to capture the near-axis peak. Much the same is true at $x = 160$ mm, with the URANS RSM calculation once more showing a dip where the data and the LES calculation show a peak. The LES calculation still overpredicts the u' levels and shows a double peak near the axis in disagreement with the experimental trends. In contrast to the previous calculations, the LES predictions of w' improve with downstream distance and by $x = 160$ mm are in remarkably good agreement with the experimental data. The poorest agreement is at $x = 10$ mm, particularly near the axis where the experiments show a peak at $r/R \approx 0.1$, whereas the calculations show an on-axis peak. It is interesting to note that for the URANS RSM calculation, the mean axial and swirling velocities show good agreement with experimental data (Figures 9 and 10), although the fluctuating values are not that good in agreement with the measurements (Figures 11 and 12). This can be explained by the above-mentioned inconsistency in the comparison of the fluctuational velocities. The displayed URANS RSM results do not consider the contributions from the unsteadily resolved velocity field. The incorporation of the latter is, unfortunately, not possible, due to the lacking information on the correlation between the resolved and modelled fluctuations. The following should serve better understanding: We can consider the (real/physical) velocity fluctuations (u') to be composed of two parts, namely a part modelled by the turbulence model, i.e. by the RSM transport equations (u'_{RSM}) and a part which is not captured by the turbulence model, but manifests itself as the unsteadiness of the computed velocity field ($u'_{UNSTEADY}$): $u' = u'_{RSM} + u'_{UNSTEADY}$. Taking square of the equation and time averaging results in:

$$\overline{u'^2} = \underbrace{\overline{u'^2_{RSM}}}_{I} + \underbrace{2\overline{u'_{RSM}u'_{UNSTEADY}}}_{II} + \underbrace{\overline{u'^2_{UNSTEADY}}}_{III}.$$

Term I on the RHS of the equation is the normal component of the Reynolds stresses, which results from the solution of the Reynolds transport equations, and which gave the basis for the displayed URANS RSM results. Contributions by Term II and Term III are missing. Term III can be calculated by monitoring the computed velocity field. The problem lies in Term II, which contains a correlation between the resolved ($u'_{UNSTEADY}$) and modelled (u'_{RSM}) fluctuational velocities, which is not known. Term II is not positive definite, and, thus, can add to or detract from the contributions of the other terms. Its order of magnitude is also quite difficult to estimate. These uncertainties have been the reason for neglecting the contributions of Term II and III in displaying the results. Still, for information, an estimation of Term III shall be given here for the axial station at $x = 10$ mm: Contributions by Term III were of comparable magnitude to those of Term I, showing deviations within a range ±10 per cent for the axial (u') and ±15 per cent for the swirl (w') fluctuational velocities. As stated above, with the lacking information on Term II, it is not possible to use this information for achieving a reliable

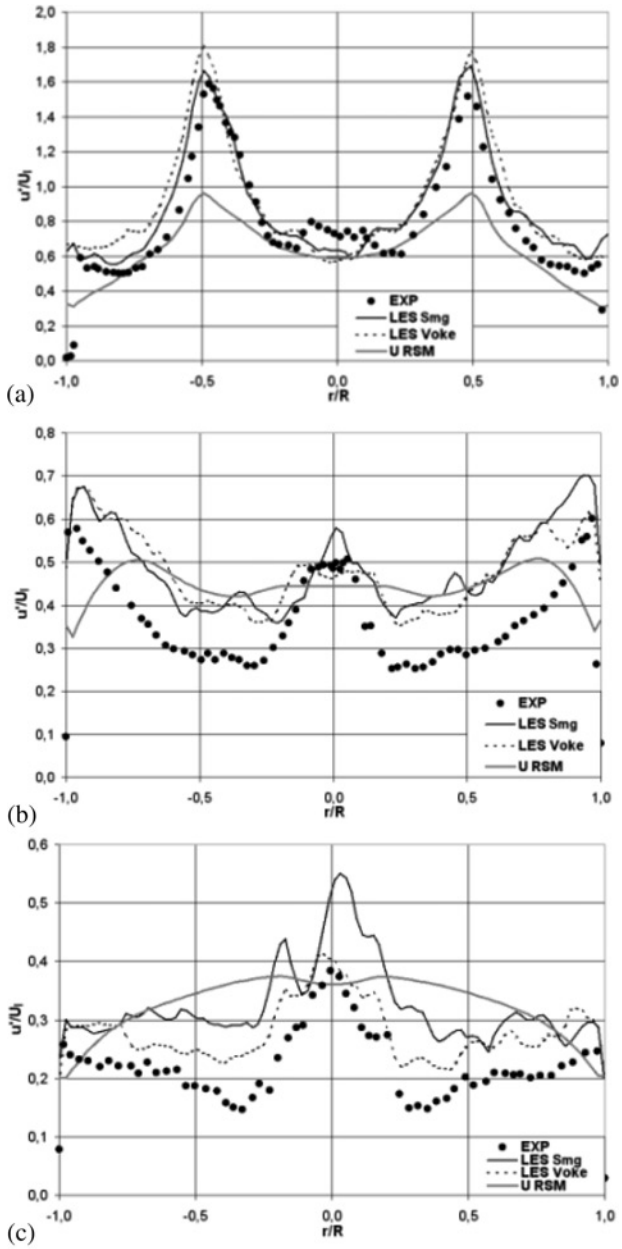

Notes: x = (a) 10 mm, (b) 50 mm and (c) 160 mm (HS)

Figure 11.
Predicted and measured radial distributions of rms fluctuations of axial velocity (u')

estimation of the physical fluctuational velocities. Cumulative contributions through the resolved velocity fluctuations (by Terms II and III) are expected to cause the present situation, where the time-averaged velocities are predicted better than the displayed fluctuational velocities.

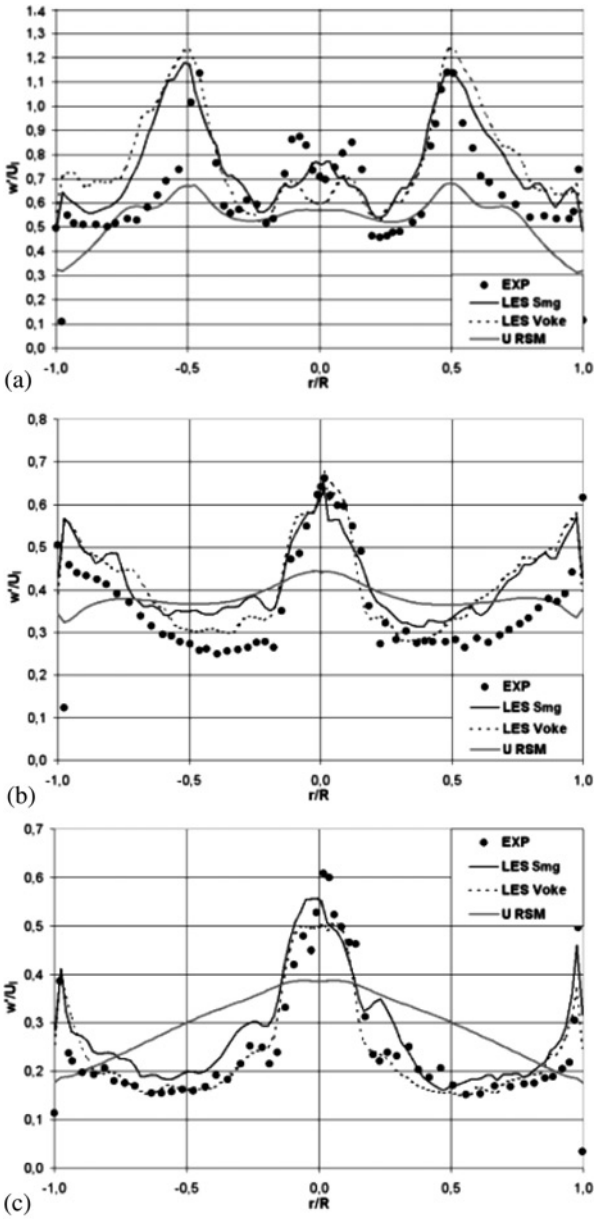

Figure 12.
Predicted and measured radial distributions of rms fluctuations of swirl velocity (w')

Notes: x = (a) 10 mm, (b) 50 mm and (c) 160 mm (HS)

5. Conclusions

Isothermal flow in an idealized swirl combustor has been investigated experimentally and computationally for a Reynolds number of 4,600 based on the bulk axial velocity and diameter at combustor inlet. Two cases are investigated, one for LS and the other for HS intensity.

The results of LDA measurements of time-averaged velocity components and corresponding rms turbulence intensities are reported for traverses at different axial locations.

The measurements are compared with numerical predictions in which LES and URANS RSM models are employed as modelling strategies. To account for the SGS turbulence in LES, models due to Smagorinsky and Voke are used. No-model LES and coarse-grid DNS computations are also performed for one of the cases. It has been observed that LES provided the best overall accuracy for all of the cases, whereas no significant differences between the Smagorinsky and Voke models are observed for the time-averaged velocity components. The relatively inferior performance of URANS RSM may be attributed to be due to rather low Reynolds number of the present flows. The observation that URANS RSM performs better for the HS case than it does for the LS one seems to support this proposition, as the turbulence levels are higher for the HS case, due to higher swirl momentum. The presently applied isotropic approximation of the anisotropic diffusion coefficients of the Reynolds stress transport equations may also be seen as a further possible cause of the observed URANS RSM behaviour.

References

ANSYS-CFX-10 (2006), *Solver Manual*, ANSYS Europe, Oxfordshire.

Barth, T.J. and Jespersen, D.C. (1989), "The design and application of upwind schemes on unstructured meshes", *AIAA 27th Aerospace Science Meeting, Reno, NV*, AIAA paper 89-0366.

Benim, A.C. and Nahavandi, A. (2003), "A computational analysis of turbulent swirling flows", in Hanjalic, K., Nagano, Y. and Tummers, M.J. (Eds), *Turbulence, Heat and Mass Transfer*, Vol. 4, Begell House, New York, NY, pp. 715-22.

Benim, A.C., Nahavandi, A. and Syed, K.J. (2005), "URANS and LES analysis of turbulent swirling flows", *Progress in Computational Fluid Dynamics*, Vol. 5, pp. 444-54.

Escudier, M.P. and Keller, J.J. (1985), "Recirculation in swirling flows: a manifestation of vortex breakdown", *AIAA Journal*, Vol. 23, pp. 111-6.

Escudier, M.P., Bornstein, J. and Zehnder, N. (1980), "Observations and LDA measurements of confined turbulent vortex flow", *Journal of Fluid Mechanics*, Vol. 98, pp. 490-63.

Fröhlich, J., Mellen, C.P., Rodi, W., Temmerman, L. and Leschziner, M.A. (2005), "Highly resolved large-eddy simulation of separated flow in a channel with streamwise periodic constrictions", *Journal of Fluid Mechanics*, Vol. 526, pp. 19-66.

Grotjans, H., Menter, F.R., Burr, R.C. and Gluck, M. (1999), "Higher order turbulence modelling in industrial applications", in Rodi, W. and Laurence, D. (Eds), *Engineering Turbulence Modelling and Experiments 4*, Elsevier, Amsterdam, pp. 269-78.

Guo, H.-F., Chen, Z.-Y. and Yu, C.-W. (2009), "3D numerical simulation of compressible swirling flow induced by means of tangential inlets", *International Journal for Numerical Methods in Fluids*, Vol. 59, pp. 1285-98.

Hinze, O.J. (1959), *Turbulence*, McGraw-Hill, New York, NY.

Hogg, S. and Leschziner, M.A. (1989), "Computation of highly swirling confined flow with a Reynolds stress turbulence model", *AIAA Journal*, Vol. 27, pp. 57-63.

Jakirlic, S., Jester-Zürker, R. and Tropea, C. (2004), "Joint effects of geometry confinement and swirling inflow on turbulent mixing in model combustors: a second-moment closure study", *Progress in Computational Fluid Dynamics*, Vol. 4, pp. 198-207.

Jawarneh, A.M. and Vatistas, G.H. (2006), "Reynolds stress model in the prediction of confined turbulent swirling flows", *ASME Journal of Fluids Engineering*, Vol. 128, pp. 1377-82.

Jones, W.P. and Launder, B.E. (1972), "The prediction of laminarisation with a two-equation model of turbulence", *International Journal of Heat and Mass Transfer*, Vol. 15, pp. 301-14.

Kawamura, T. and Kuwahara, K. (1984), "Computation of high Reynolds number flow around a circular cylinder with surface roughness", AIAA Paper 84-0340.

Kim, W.-W, Menon, S. and Mongia, H.C. (1999), "Large-eddy simulation of a gas turbine combustor flow", *Combustion Science and Technology*, Vol. 143, pp. 25-62.

Launder, B.E. and Sharma, B.T. (1974), "Application of the energy dissipation model of turbulence to the calculation of flow near a spinning disc", *Letters in Heat and Mass Transfer*, Vol. 1, pp. 131-8.

Launder, B.E. and Spalding, D.B. (1974), "The numerical computation of turbulent flows", *Computer Methods in Applied Mechanics and Engineering*, Vol. 3, pp. 269-89.

Launder, B.E., Reece, G.J. and Rodi, W. (1975), "Progress in the development of a Reynolds-stress turbulence closure", *Journal of Fluid Mechanics*, Vol. 68, pp. 537-66.

Pao, Y.-H. (1965), "Structure of turbulent velocity and scalar fields at large wave numbers", *Physics of Fluids*, Vol. 8, pp. 1063-75.

Peyret, R. (Ed.) (2000), *Handbook of Computational Fluid Dynamics*, Academic Press, San Diego, CA.

Sagaut, P. (2002), *Large Eddy Simulation for Incompressible Flows – An Introduction*, 2nd ed., Springer Verlag, Berlin.

Sagaut, P., Comte, P. and Ducros, F. (2000), "Filtered subgrid-scale models", *Physics of Fluids*, Vol. 12, pp. 233-6.

Selle, L., Lattigue, G., Poinsot, T., Koch, R., Schildmacher, U. and Krebs, W. (2004), "Compressible large-eddy simulations of turbulent combustion in a complex geometry on unstructured meshes", *Combustion and Flame*, Vol. 137, pp. 489-505.

Shih, T.-H., Liou, W.W., Shabbir, A. and Zhu, J. (1995), "A new k-ε eddy-viscosity model for high Reynolds number turbulent flows – model development and validation", *Computers and Fluids*, Vol. 24, pp. 227-38.

Sloan, D.G., Smith, P.J. and Smoot, L.D. (1986), "Modelling of swirl in turbulent flow systems", *Progress in Energy and Combustion Science*, Vol. 12, pp. 163-250.

Smagorinsky, J. (1963), "General circulation experiments with the primitive equations. I: the basic experiment", *Monthly Weather Review*, Vol. 91, pp. 99-164.

Speziale, C.G., Sarkar, S. and Gatski, T.B. (1991), "Modelling the pressure-strain correlation of turbulence", *Journal of Fluid Mechanics*, Vol. 227, pp. 245-72.

Van Driest, E.R. (1956), "On turbulent flow near a wall", *Journal of Aeronautical Science*, Vol. 23, pp. 1007-11.

Voke, P.R. (1996), "Subgrid-scale modelling at low mesh Reynolds number", *Theoretical Computation in Fluid Dynamics*, Vol. 8, pp. 131-43.

Weber, R., Visser, B.M. and Boysan, F. (1990), "Assessment of turbulence modelling for engineering prediction of swirling vortices in the near burner zone", *International Journal of Heat and Fluid Flow*, Vol. 11, pp. 225-35.

Xia, J.L., Smith, B.L., Benim, A.C., Schmidli, J. and Yadigaroglu, G. (1997), "Effect of inlet and outlet boundary conditions on swirling flows", *Computers and Fluids*, Vol. 26, pp. 811-23.

Yaras, M.I. and Grosvenor, A.D. (2003), "Evaluation of one- and two-equation low-Re turbulence models. Part I – axisymmetric separating and swirling flows", *International Journal of Numerical Methods in Fluids*, Vol. 42, pp. 1293-19.

Corresponding author
A.C. Benim can be contacted at: alicemal.benim@fh-duesseldorf.de